

Mechanisms of $[Ca^{2+}]_i$ Transient Decrease in Cardiomyopathy of *db/db* Type 2 Diabetic Mice

Laetitia Pereira,¹ Jan Matthes,² Iris Schuster,³ Héctor H. Valdivia,⁴ Stefan Herzig,² Sylvain Richard,¹ and Ana M. Gómez¹

Cardiovascular disease is the leading cause of death in the diabetic population. However, molecular mechanisms underlying diabetic cardiomyopathy remain unclear. We analyzed Ca^{2+} -induced Ca^{2+} release and excitation-contraction coupling in *db/db* obese type 2 diabetic mice and their control littermates. Echocardiography showed a systolic dysfunction in *db/db* mice. Two-photon microscopy identified intracellular calcium concentration ($[Ca^{2+}]_i$) transient decrease in cardiomyocytes within the whole heart, which was also found in isolated myocytes by confocal microscopy. Global $[Ca^{2+}]_i$ transients are constituted of individual Ca^{2+} sparks. Ca^{2+} sparks in *db/db* cardiomyocytes were less frequent than in $+/+$ myocytes, partly because of a depression in sarcoplasmic reticulum Ca^{2+} load but also because of a reduced expression of ryanodine receptor Ca^{2+} channels (RyRs), revealed by [³H]ryanodine binding assay. Ca^{2+} efflux through Na^+/Ca^{2+} exchanger was increased in *db/db* myocytes. Calcium current, I_{Ca} , triggers sarcoplasmic reticulum Ca^{2+} release and is also involved in sarcoplasmic reticulum Ca^{2+} refilling. Macroscopic I_{Ca} was reduced in *db/db* cells, but single Ca^{2+} channel activity was similar, suggesting that diabetic myocytes express fewer functional Ca^{2+} channels, which was confirmed by Western blots. These results demonstrate that *db/db* mice show depressed cardiac function, at least in part, because of a general reduction in the membrane permeability to Ca^{2+} . As less Ca^{2+} enters the cell through I_{Ca} , less Ca^{2+} is released through RyRs. *Diabetes* 55:608–615, 2006

Diabetes prevalence is rising in Western countries and affects ~143 million patients worldwide, thus approximately five times surpassing estimations made a decade ago (1). About 90% of diabetic patients exhibit non-insulin-dependent (or insulin-resistant) type 2 diabetes, and at least 80% of type 2 diabetic patients in Western countries are obese. These

patients usually exhibit severe glucose intolerance compared with lean type 2 diabetic patients (2). Cardiovascular disease is the leading cause of death in the diabetic population (3–5). Although cardiovascular problems could be the result of associated comorbidities, a defect in cardiac performance has been detected in diabetic patients in the absence of vascular injury, supporting the existence of a specific diabetic cardiomyopathy. Reductions in diastolic compliance, contractility, and rate of myocardial relaxation characterize diabetic cardiomyopathy (6–8). However, cellular and molecular bases of cardiac dysfunction are largely unknown in type 2 diabetes.

Because Ca^{2+} release and uptake are at the root of contraction and relaxation, alteration of Ca^{2+} handling has been suspected to drive the progression of functional abnormalities in diseased hearts. However, data regarding Ca^{2+} handling in type 2 diabetes are limited and ambiguous. For example, a rat model of insulin-resistant obese type 2 diabetes (cp/cp) shows enhanced Ca^{2+} uptake into sarcoplasmic reticulum, but sarcoplasmic reticulum Ca^{2+} ATPase (SERCA) levels and sarcoplasmic reticulum Ca^{2+} load are unaltered (9). By contrast, other well-known models of type 2 diabetes such as Otsuka Long Evans Tokushima Fatty rats (10) and *db/db* mice (11) present defects in both function and expression of SERCA. Streptozotocin injection in neonatal rats induces adult non-insulin-dependent diabetes, and the activities of plasmalemmal Ca^{2+} ATPase (12,13) and Na^+/Ca^{2+} exchanger (NCX) (13) are both decreased in this model. Thus, a distinct Ca^{2+} transporter malfunction has been identified in different diabetic models, but an integrated mechanism of altered Ca^{2+} homeostasis is lacking.

We characterized Ca^{2+} -induced Ca^{2+} release and excitation-contraction coupling in hearts of *db/db* mice, an obesity-linked mouse model of type 2 diabetes. Like humans with diabetic cardiomyopathy, *db/db* mice display increased left ventricular end-diastolic pressure, decreased left ventricular systolic pressure at high preload, and lowered cardiac output (14). We found impaired intracellular calcium concentration ($[Ca^{2+}]_i$) cycling that may explain these functional changes: a reduction in L-type calcium current I_{Ca} underlies a reduction in $[Ca^{2+}]_i$ transient and contraction, both of which are exacerbated by a decrease in ryanodine receptor Ca^{2+} channel (RyR) density and sarcoplasmic reticulum Ca^{2+} load.

RESEARCH DESIGN AND METHODS

M-mode echocardiography. Fifteen-week-old male and female C57BL/KsJ-*db* (*db/db*) mice and their control littermates ($+/+$) were used. All experiments were carried out according to the ethical principles laid down by the French Ministry of Agriculture and European Union Council Directives for

From the ¹Institut National de la Santé et de la Recherche Médicale, U 637, University of Montpellier 1, Montpellier, France; the ²Department of Pharmacology and Center of Molecular Medicine, University of Cologne, Cologne, Germany; the ³School of Medicine, University of Montpellier 1, EA 2992, Nîmes, France; and the ⁴Department of Physiology, University of Wisconsin Medical School, Madison, Wisconsin.

Address correspondence and reprint requests to Ana María Gómez, Institut National de la Santé et de la Recherche Médicale U-637, CHU A. de Villeneuve, 34295 Montpellier, France. E-mail: agomez@montp.inserm.fr.

Received for publication 3 October 2005 and accepted in revised form 30 November 2005.

$[Ca^{2+}]_i$, intracellular calcium concentration; NCX, Na^+/Ca^{2+} exchanger; RyR, ryanodine receptor Ca^{2+} channel; SERCA, sarcoplasmic reticulum Ca^{2+} ATPase.

© 2006 by the American Diabetes Association.

The costs of publication of this article were defrayed in part by the payment of page charges. This article must therefore be hereby marked "advertisement" in accordance with 18 U.S.C. Section 1734 solely to indicate this fact.

the care of laboratory animals. Transthoracic echocardiography was performed in anesthetized animals (35 mg/kg sodium pentobarbital) using an ultrasound machine (Esaote "Mylab", Florence, Italy) and a 10-MHz phase-array transducer. Parameters were determined using the leading-edge method of the American Society of Echocardiography. End-diastole was determined at the maximal left ventricular diastolic dimension, and end-systole was taken at the peak of posterior wall motion. Systolic function was calculated as fractional shortening: % fractional shortening = (left ventricular end-diastolic dimension - left ventricular end-systolic dimension)/left ventricular end-diastolic dimension \times 100. Heart rate was determined from measurements of cardiac cycle length on spectral Doppler tracings of the aortic outflow. All data are the average of at least three separate scans, each scan representing the average of three consecutive beats.

Two-photon microscopy in whole hearts. At the time of the experiments, mice were weighed and anesthetized with sodium pentobarbital (100 mg/kg i.p.). The heart was quickly removed and weighed. The aorta was cannulated, and the heart was perfused with a HEPES-based Tyrode solution and used for two-photon microscopy. First, the heart was perfused \sim 15 min with a solution similar to that used for cell isolation (15) but supplemented with 1.8 mmol/l CaCl_2 and 50 mmol/l butanedione monoxime (16) to prevent contraction. Then, the same solution containing the fluorescence Ca^{2+} dye Rhod-2 AM (10 $\mu\text{mol/l}$; Teflabs) was perfused for 20 min. After this loading time, the same solution free of Rhod-2 and of butanedione monoxime and supplemented with 50 $\mu\text{mol/l}$ cytochalasin D to block contractions was perfused throughout the experiment. After 20–30 min, the heart was placed on the stage of an upright microscope (Axioskop 2FSmot Meta LSM510, adapted for two-photon microscopy, ceramic objective IR40 \times , numerical aperture 0.8; Zeiss) under continuous perfusion. The hearts were electrically stimulated through a bipolar platinum electrode at 2 Hz. Ca^{2+} images were obtained with illumination supplied by a mode-locked Ti:Sapphire laser (Mira 900; Coherent) tuned to a center wavelength of 820 nm. Emission was collected at $>$ 560 nm wavelength. $[\text{Ca}^{2+}]_i$ transients were recorded in the line-scan mode at 3 ms/line. To visualize cell membranes, the heart was loaded with the voltage-sensitive dye di-4 ANEPPS in a single bolus (16), and three-dimensional images were recorded with the two-photon microscope.

Isolated cells. Ventricular myocytes were isolated from $+/+$ and db/db mice as previously described (15). Whole-cell patch clamp (Axopatch 200A; Axon Instruments) was used to monitor L-type Ca^{2+} currents (I_{Ca}). The patch pipette contained 50 $\mu\text{mol/l}$ Fluo-3 pentapotassium salt to simultaneously record the associated $[\text{Ca}^{2+}]_i$ transient. Voltage protocol and solutions were as previously described (17). $[\text{Ca}^{2+}]_i$ transients were recorded with the confocal microscope (MetaZeiss LSM510, objective water immersion \times 60, numerical aperture 1.2) in line-scan mode (1.5 ms/line). The 488-nm line of the argon laser was used to illuminate, and emission was collected at $>$ 505 nm. The line of scan was selected parallel to the longitudinal cell axis to measure cell shortening.

Sarcoplasmic reticulum Ca^{2+} load was estimated by rapid caffeine application to isolated cells. Myocytes were previously depolarized to 0 mV (150-ms steps) from a holding potential of -80 mV for 1 min, then 10 mmol/l caffeine was added, and the associated fluorescence image was recorded by confocal microscopy. In some cells, the associated NCX current was recorded by patch clamp and integrated to estimate the amount of Ca^{2+} released by the sarcoplasmic reticulum (18). Ca^{2+} sparks were recorded in saponin-permeabilized myocytes as previously described (19) using an internal solution containing 50 nmol/l free Ca^{2+} . Image analyses were done using homemade routines in IDL (interactive data language) (RSI) (20). All experiments performed on isolated hearts or myocytes were carried out at room temperature (21–23°C).

Single-channel recording. Cardiomyocytes were placed in a depolarizing solution containing 120 mmol/l potassium glutamate, 25 mmol/l KCl, 2 mmol/l MgCl_2 , 10 mmol/l HEPES, 2 mmol/l EGTA, 1 mmol/l CaCl_2 , 1 mmol/l Na_2ATP , and 10 mmol/l glucose (pH 7.4 with KOH). Borosilicate pipettes (5–12 M Ω) were coated with Sylgard and filled with a solution containing 70 mmol/l BaCl_2 , 90 mmol/l sucrose, and 10 mmol/l HEPES (pH 7.4 with TEA-OH). Ba^{2+} currents carried by single L-type Ca^{2+} channels were recorded using the cell-attached configuration of the patch-clamp technique as previously described (21), applying voltage steps to $+20$ mV from a holding potential of -100 mV, at least 180 sweeps per experiment. Data were sampled at 10 KHz and filtered at 2 KHz using an Axopatch 200A amplifier and analyzed with pClamp6 software (Axon Instruments). In case of multichannel patches, all data were corrected by the number of channels as described previously (22). **$[\text{^3H}]$ ryanodine binding assay.** Hearts were homogenized in a buffer containing 30 mmol/l KH_2PO_4 , 20 mmol/l NaF, 300 mmol/l sucrose, 0.012 mmol/l leupeptin, 0.1 mmol/l phenylmethylsulfonyl fluoride, and 0.01 mmol/l benzamide (pH 7 with NaOH). Insoluble material was removed by centrifugation at 1,000 rpm for 1 min (4°C). Protein quantification was done with the Bradford assay using BioRad reagents. The $[\text{^3H}]$ ryanodine binding assay was

performed as described previously (23) using 20 μg heart protein homogenate/assay tube in a buffer containing 1 mol/l NaCl, 50 $\mu\text{mol/l}$ CaCl_2 , and 20 mmol/l Na-PIPES, pH 7.2. B_{max} , the maximal number of receptor sites, and K_d , the affinity constant of the receptor-ligand interaction, were obtained by fitting data points with the formula $B = B_{\text{max}} \times [\text{^3H}]$ ryanodine / ($K_d + [\text{^3H}]$ ryanodine), where B is the specific binding. Nonspecific binding was determined in the presence of 20 $\mu\text{mol/l}$ ryanodine.

Western blot. Ventricular protein homogenates were made as described previously (21). Ventricles were rapidly frozen in liquid nitrogen and then placed in Tris solution (50 mmol/l, pH 7.4) containing 1 mmol/l phenylmethylsulfonyl fluoride and chopped using an Ultra-Turrax disperser. Suspension was centrifuged for 15 min (3,500 $\times g$). Supernatant was then centrifuged for 60 min (55,000 $\times g$). The pellet was dissolved in 50 mmol/l Tris solution (pH 6.8) containing 2% (wt/vol) SDS, 20% glycerol, and 5 mmol/l dithiothreitol. After shaking for 30 min, probes were frozen at -80°C until subjecting to SDS-PAGE on 8% running gel and 5% stacking gel. For protein analysis, equal amounts of 15 μg per probe were used. SDS-PAGE was blotted to polyvinylidene fluoride membranes (Bio-Rad) by using a semidry Western-blot system. $\text{Ca}_v1.2$ ($\alpha 1\text{C}$) proteins were detected by a specific antibody (C-1603; dilution, 1:600; Sigma-Aldrich) using alkaline-phosphatase reaction. Protein bands were analyzed densitometrically.

Data analysis. Male and female animals were used in an attempt to identify sex differences in the diabetic cardiomyopathy (4). However, because no difference was found, both male and female data were pooled together. Data are presented as means \pm SE, and t test was used to compare data obtained in $+/+$ and db/db mice. $P < 0.05$ was considered statistically significant.

RESULTS

db/db mice hearts are functionally defective but not hypertrophied. Echocardiography confirmed functional impairment of db/db hearts (Fig. 1A). Decreased shortening fraction in db/db mice indicated contractile dysfunction (Fig. 1B), whereas left ventricular wall thickness was similar in $+/+$ and db/db mice (Table 1). Heart weight was similar for both groups (Fig. 1C). To assess hypertrophy of cardiomyocytes, we measured cell dimensions in hearts loaded with the voltage-sensitive dye di-4 ANEPPS, which labels the external cell membrane, and three-dimensional images were recorded. Deconvolution was applied with Huygens (Bitplane) to correct for thickness distortion (24). A deconvoluted two-photon image of cell membranes is shown in Fig. 1D. In agreement with unchanged cell capacitance (Table 1), calculated cell volume was not altered (Fig. 1E).

Cellular $[\text{Ca}^{2+}]_i$ transients recorded in whole hearts. To determine whether altered cellular Ca^{2+} signaling underlies this cardiac dysfunction, we recorded $[\text{Ca}^{2+}]_i$ transients in whole hearts. Freshly explanted hearts were loaded with Rhod-2 (Fig. 1F) and electrically evoked $[\text{Ca}^{2+}]_i$ transients in individual myocytes were visualized with two-photon microscopy in the line-scan mode. Figure 1G shows representative images of a $+/+$ cell (*top*), of a db/db cell (*middle*), and the corresponding calculated $[\text{Ca}^{2+}]_i$ transients (*bottom*). The $[\text{Ca}^{2+}]_i$ transients recorded in db/db cells were smaller in amplitude and decayed more slowly. Averaged data (Fig. 1H) indicate a significant reduction of $[\text{Ca}^{2+}]_i$ transient amplitude in db/db myocytes compared with $+/+$ myocytes. The duration of $[\text{Ca}^{2+}]_i$ transient at half-maximum amplitude, D_{50} , was significantly longer ($P < 0.01$) in db/db myocytes (176.9 ± 5.4 ms) than in $+/+$ cells (104.1 ± 2.4 ms). Thus, db/db hearts have depressed contractile properties and decreased $[\text{Ca}^{2+}]_i$ transients but with no apparent remodeling of the heart. To characterize impairment of $[\text{Ca}^{2+}]_i$ transients in more detail, we analyzed the function and expression of L-type Ca^{2+} channels and RyRs and measured sarcoplasmic reticulum Ca^{2+} load, thus examining critical steps in cardiac Ca^{2+} cycling more comprehensively.

TABLE 1
Characteristics of +/+ and *db/db* mice

	Body weight (g)	Heart weight (mg)	Cm (pF)	LVEDD (mm)	LVESD (mm)	FS (%)	SWT (mm)	PWT (mm)	HR (bpm)
+/+	22.3 ± 0.8 (17)	171 ± 7 (17)	153 ± 7 (62)	3.1 ± 0.1 (3)	1.2 ± 0.1 (3)	60.6 ± 1.9 (3)	0.7 ± 0.7 (3)	0.7 ± 0.1 (3)	241 ± 18 (3)
<i>db/db</i>	49.3 ± 1.1 (30)*	184 ± 7 (29)	169 ± 7 (53)	3.5 ± 0.1 (3)†	2.3 ± 0.2 (3)*	33.7 ± 5.6 (3)*	0.7 ± 0.1 (3)	0.7 ± 0.1 (3)	238 ± 11 (3)

Data are means ± SE (*n*). Cm, membrane capacitance; FS, fractional shortening; HR, heart rate; LVEDD, left ventricular end-diastolic diameter; LVESD, left ventricular end-systolic diameter; PWT, posterior wall thickness; SWT, septal wall thickness. **P* < 0.001; †*P* < 0.05.

L-type Ca²⁺ channels and excitation-contraction coupling. Ca²⁺ release from the sarcoplasmic reticulum is graded by *I*_{Ca}, the “trigger” current carried by L-type Ca²⁺ channels. We thus recorded whole-cell *I*_{Ca} in single myocytes. *I*_{Ca} was significantly decreased in *db/db* myocytes compared with controls (+/+) (Fig. 2A and D). To determine the *I*_{Ca}-sarcoplasmic reticulum Ca²⁺ release coupling efficiency, we simultaneously recorded *I*_{Ca} and its triggered [Ca²⁺]_i transient by confocal microscopy. Consistent with reduced [Ca²⁺]_i transients observed in single cells within the whole hearts, [Ca²⁺]_i transients were decreased and slowed in isolated *db/db* cells as well. Figure 2C is a plot of peak [Ca²⁺]_i transient (*F*/*F*₀, with *F*, the fluorescence signal, and *F*₀, the diastolic fluorescence) as a function of voltage step in *db/db* and +/+ cells. The decay time of the [Ca²⁺]_i transient, calculated by fitting the decay phase of the fluorescence signal to a mono-exponential function, was prolonged in *db/db* myocytes (decay time constant at 0 mV, 160.1 ± 8.1 ms in 38 +/+ cells vs. 192.7 ± 12.4 ms in 16 *db/db* myocytes; *P* < 0.05). The reduction of sarcoplasmic reticulum Ca²⁺ release in *db/db* myocytes obviously paralleled the decrease of whole-cell *I*_{Ca}. Accordingly, cell contraction, which steeply follows the magnitude of the [Ca²⁺]_i transient (25), was significantly reduced in *db/db* cells at most potentials (Fig. 2B). Cell shortening, as shown in Fig. 2A (lower traces), was also slowed in diabetic myocytes. Maximum derivative over time (dL/dt) at 0 mV (in % cell length/ms) was 0.33 ± 0.03 in +/+ cells vs. 0.21 ± 0.03 in *db/db* cells (*P* < 0.05). To estimate excitation-contraction coupling gain, we normalized Ca²⁺ release (amplitude of [Ca²⁺]_i transient) by total Ca²⁺ entry (integral of *I*_{Ca}) and plotted it as a function of voltage (Fig. 2E). *db/db* and +/+ myocytes showed similar excitation-contraction coupling gain, indicating that the efficacy of *I*_{Ca} to trigger Ca²⁺ release remains unchanged in *db/db* myocytes.

The decrease of macroscopic *I*_{Ca} could be due to altered voltage dependence, impaired single-channel gating, or decreased expression of L-type Ca²⁺ channels. We first analyzed steady-state activation and inactivation of *I*_{Ca}. Figure 3A shows that steady-state inactivation curves in +/+ (solid line and open symbols) and *db/db* (dotted line and filled symbols) were not different regarding half-inactivation potential (*V*_{1/2}: -33.1 ± 1.5 mV for +/+, *n* = 17 vs. -31.6 ± 1.1 mV for *db/db*, *n* = 11; *P* > 0.05) or slope factor (5.53 ± 0.31 for +/+, *n* = 17 vs. 5.44 ± 0.54 for *db/db*, *n* = 11; *P* > 0.05). Steady-state activation was slightly shifted toward more depolarized potentials in *db/db* myocytes (dotted line) compared with +/+ myocytes (solid line) (-17.0 ± 0.7 mV in +/+ cells, *n* = 43 vs. -13.8 ± 0.8 mV, *n* = 20; *P* < 0.01) without alteration of the slope factor (4.95 ± 0.29 in +/+ cells vs. 4.81 ± 1.19 in *db/db*).

Reduction of *I*_{Ca} may reflect altered single-channel properties and/or decreased number of functional channels in the membrane. Recording of single L-type Ca²⁺ channels (Fig. 3B) revealed no difference regarding fraction of active sweeps (46 ± 8 vs. 44 ± 3% in six +/+ vs. five *db/db* patches, respectively) and mean open time (0.61 ± 0.05 vs. 0.58 ± 0.02 ms in +/+ vs. *db/db*, respectively), open probability in active sweeps (+/+, 14.3 ± 4.2%; *db/db*, 21.3 ± 4.5%), and peak ensemble average currents (Fig. 3B, bottom panels) (-77 ± 23 fA in +/+ vs. -82 ± 17 fA in *db/db*) obtained with *db/db* (*n* = 5 patches) or +/+ (*n* = 6 patches) myocytes. Thus, the activity of single L-type Ca²⁺ channels was un-

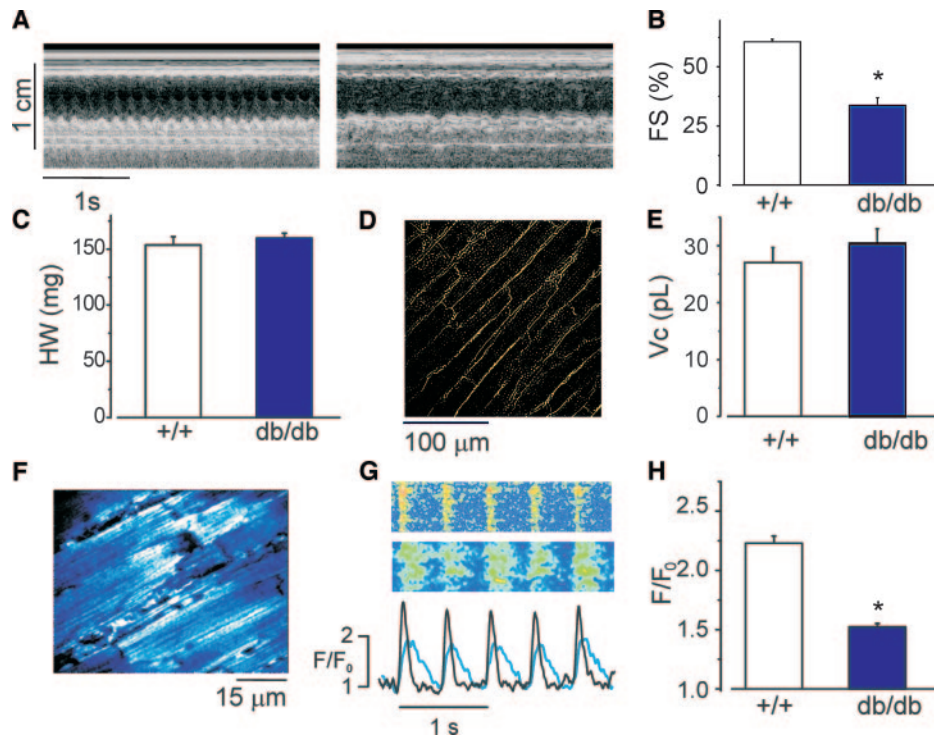


FIG. 1. *db/db* mice show cardiac dysfunction associated with decreased $[Ca^{2+}]_i$ transients but lack signs of cardiac hypertrophy. **A:** M-mode echocardiographic images obtained in +/+ (left) and *db/db* mouse (right). **B:** Fractional shortening in +/+ ($n = 3$) and *db/db* ($n = 3$) mice. **C:** +/+ and *db/db* heart weight. **D:** Deconvoluted two-photon image in a mouse heart loaded with di-4 ANEPPS. **E:** Cell volumes in +/+ ($n = 40$) and *db/db* mice ($n = 66$). **F:** Two-photon image of mouse heart loaded with Rhod-2 AM. **G:** Examples of two-photon line-scan images recorded in hearts loaded with Rhod-2 AM in cell from +/+ (top) and *db/db* heart (middle). Corresponding $[Ca^{2+}]_i$ transients (expressed as F/F_0) are superimposed at the bottom. Black trace, +/+ cell. Blue trace, *db/db* cell. Hearts were paced at 2 Hz. **H:** Averaged values of peak F/F_0 in +/+ (113 cells from five hearts) and *db/db* (77 cells from four hearts). * $P < 0.0001$.

changed. These findings suggest that the 31.2% decrease in macroscopic I_{Ca} may reflect lower expression of channel proteins. To test this possibility, we carried out Western-blot analysis of $Ca_v1.2$, the pore-forming $\alpha 1C$

subunit of L-type Ca^{2+} channels (Fig. 3C). In agreement with the decrease in whole-cell I_{Ca} , the expression of $\alpha 1C$ protein was reduced by $\sim 38\%$ in *db/db* ventricles (Fig. 3C).

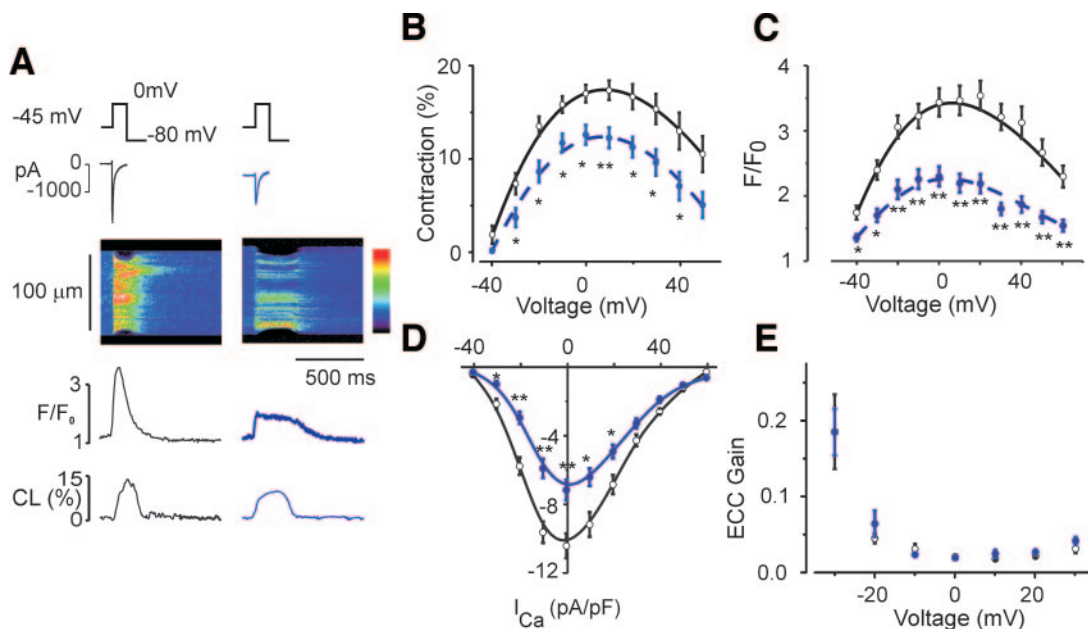


FIG. 2. *db/db* mice exhibit depressed $[Ca^{2+}]_i$ transients due to I_{Ca} decrease. **A:** Example recordings taken from +/+ cell (left) and *db/db* cell (right). From top to bottom: voltage protocol, I_{Ca} line-scan confocal image, fluorescence trace, and shortening trace (CL%, percentage of cell length). **B:** Cell shortening as a function of voltage in +/+ (open circle and solid line, $n = 20$) and *db/db* cells (blue circle and dashed line, $n = 11$). **C:** Peak $[Ca^{2+}]_i$ transient (F/F_0 , see Fig. 1) plotted against voltage in +/+ ($n = 44$) and *db/db* ($n = 20$) myocytes. Symbols as in B. **D:** I_{Ca} density plotted against voltage in +/+ and *db/db* cells. Symbols and number of samples as in C. **E:** Plot of excitation-contraction coupling gain calculated for each voltage dividing the F/F_0 by the integral of I_{Ca} (pC/pF). Open circles, +/+ cells; blue circles, *db/db* cells. * $P < 0.05$; ** $P < 0.005$.

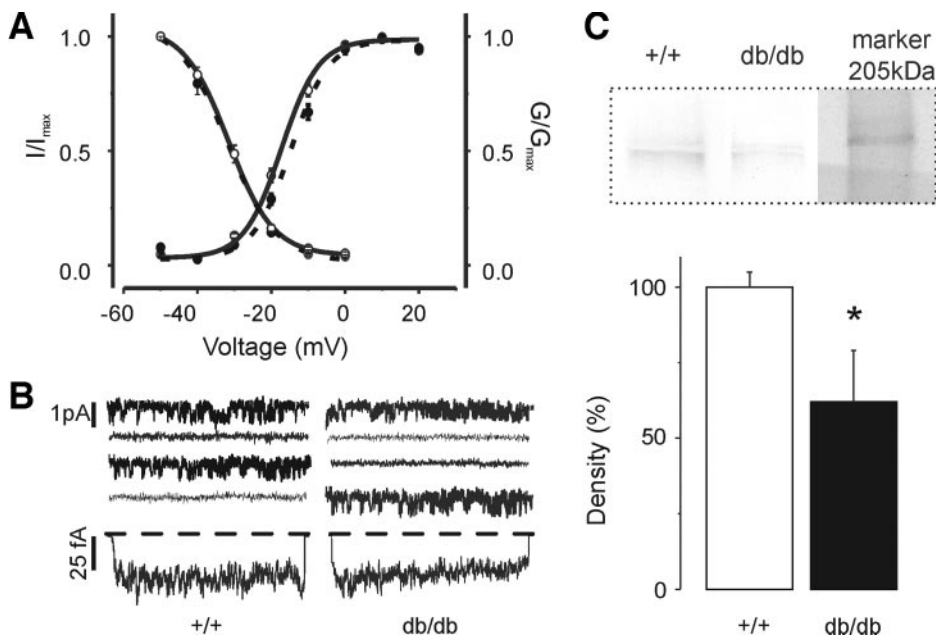


FIG. 3. Biophysical properties of the calcium current. *A:* Steady-state activation and inactivation curves obtained from -60 to $+20$ mV for +/+ (\circ and solid line, $n = 6$) and *db/db* (\bullet and dashed line, $n = 5$). *B:* Consecutive traces obtained from single-channel recordings within +/+ (left) and *db/db* (right). Traces were obtained during 150-ms depolarization steps from -100 to $+20$ mV. Bottom traces are ensemble currents obtained in each experiment. *C:* Top: Representative Western blot of +/+ and *db/db* samples from ventricular tissue homogenates; bottom: statistical analysis of *db/db* ($n = 5$) and +/+ hearts ($n = 6$) (* $P < 0.05$).

RyR activity and abundance. The opening of a RyR cluster produces local, rapid, and brief elevations in $[\text{Ca}^{2+}]_i$ termed Ca^{2+} sparks (26). Ca^{2+} sparks occur spontaneously during diastole and are activated during systole by I_{Ca} . To avoid the compounding effect of I_{Ca} , we analyzed Ca^{2+} sparks in saponin-permeabilized myocytes. In the absence of external membrane control, the excitation-contraction coupling machinery is reduced to Ca^{2+} release by RyR and Ca^{2+} uptake by SERCA2a, thus allowing direct assessment of these parameters. Moreover, permeabilized cells allow easy clamping of internal $[\text{Ca}^{2+}]_i$, so that Ca^{2+} uptake and release in +/+ and *db/db* cells may be determined under identical conditions. Figure 4A shows confocal line-scan images in a +/+ (top) and a *db/db* (bottom) myocyte, which exhibited fewer Ca^{2+} sparks. The averaged Ca^{2+} spark frequency recorded in *db/db* myocytes was reduced in diabetic myocytes (Fig. 4B). An analysis of RyR expression by [^3H]ryanodine binding to cardiac homogenates (Fig. 4C) revealed that B_{\max} was decreased in *db/db* hearts (Fig. 4D) (0.10 ± 0.01 pmol/mg protein) compared with +/+ hearts (0.16 ± 0.02 pmol/mg protein), whereas K_d , the RyR- $[\text{H}^3]$ ryanodine affinity constant, was similar (3.7 ± 1.1 and 4.4 ± 0.8 nmol/l in +/+ and *db/db* hearts, respectively). Thus, a reduction in RyR expression levels may contribute, at least in part, to the decrease in Ca^{2+} spark occurrence observed in permeabilized cells.

Sarcoplasmic reticulum Ca^{2+} load. Sarcoplasmic reticulum Ca^{2+} load is a major determinant of Ca^{2+} release and, by extension, a critical factor in Ca^{2+} spark frequency and $[\text{Ca}^{2+}]_i$ transient amplitude. It is plausible, therefore, that sarcoplasmic reticulum Ca^{2+} load contributes to the decrease in both amplitude of $[\text{Ca}^{2+}]_i$ transient (Figs. 1H and 2C) and Ca^{2+} spark frequency (Fig. 4B) observed in *db/db* hearts, independently or in combination with the decreased expression of L-type Ca^{2+} channels and RyRs. We thus measured sarcoplasmic reticulum Ca^{2+} content after caffeine application in conditions used to record Ca^{2+} sparks and $[\text{Ca}^{2+}]_i$ transients, i.e., in permeabilized and intact myocytes, respectively. Two examples of line-scan images recorded during caffeine application in permeabilized myocytes and the average data are displayed in

Fig. 4E. Permeabilized *db/db* myocytes have lower sarcoplasmic reticulum Ca^{2+} content, suggesting a decreased activity of SERCA pump. We also estimated sarcoplasmic reticulum Ca^{2+} load by rapid caffeine application to non-permeabilized myocytes. Figure 5A shows examples of line-scan images recorded in a +/+ (top) and a *db/db* (bottom) myocyte. The caffeine-evoked $[\text{Ca}^{2+}]_i$ transient was smaller in *db/db* myocyte, as demonstrated by the averaged data in Fig. 5B. The caffeine-evoked $[\text{Ca}^{2+}]_i$ transient activates the forward-mode of the NCX, eliciting an inward current as Ca^{2+} is extruded. Hence, the integral of the inward NCX current is a reliable index of the sarcoplasmic reticulum Ca^{2+} load (18). Figure 5C shows examples of NCX currents (left) and their running integrals (right) in a +/+ (top) and a *db/db* (bottom) cell. Figure 5D shows the averaged data of the integral of the caffeine-evoked NCX current and confirms the reduction of sarcoplasmic reticulum Ca^{2+} load in *db/db* myocytes. Thus, a reduction in sarcoplasmic reticulum Ca^{2+} load may contribute, in combination with decreased expression of RyRs and L-type Ca^{2+} channels, to the decrease in Ca^{2+} spark frequency and $[\text{Ca}^{2+}]_i$ transient amplitude and may be a major determinant of the contractile dysfunction of diabetic hearts.

The diminution in sarcoplasmic reticulum Ca^{2+} load may reflect decreased Ca^{2+} entry through I_{Ca} and slowing in sarcoplasmic reticulum Ca^{2+} uptake but also increased efflux through the NCX. In many models of heart failure, the NCX current (I_{NCX}) is increased (27). We measured peak I_{NCX} (pA) activated by the increase in $[\text{Ca}^{2+}]_i$ (F/F_0) at a membrane potential of -80 mV and found that I_{NCX} is increased in *db/db* myocytes (in $\text{pA}/[F/F_0]$, 27.6 ± 2.6 in 20 +/+ cells vs. 47.9 ± 7.2 in 20 *db/db* cells, $P < 0.05$). In heart failure after myocardial infarction, we found that although the I_{NCX} was increased, there was a concomitant increase in cell volume that cancels out the relative increase of I_{NCX} , thus unaltering the capacity of the cell to extrude Ca^{2+} (28). We therefore normalized I_{NCX} by $[\text{Ca}^{2+}]_i$ and by cell volume. We found that I_{NCX} (pA) normalized by $[\text{Ca}^{2+}]_i$ (F/F_0) and by cell volume (pL) was 1.0 ± 0.1 in +/+ myocytes ($n = 20$) and 1.6 ± 0.2 in *db/db* ($n = 20$), $P < 0.05$. So *db/db* myocytes show an increased $[\text{Ca}^{2+}]_i$ efflux for a given $[\text{Ca}^{2+}]_i$.

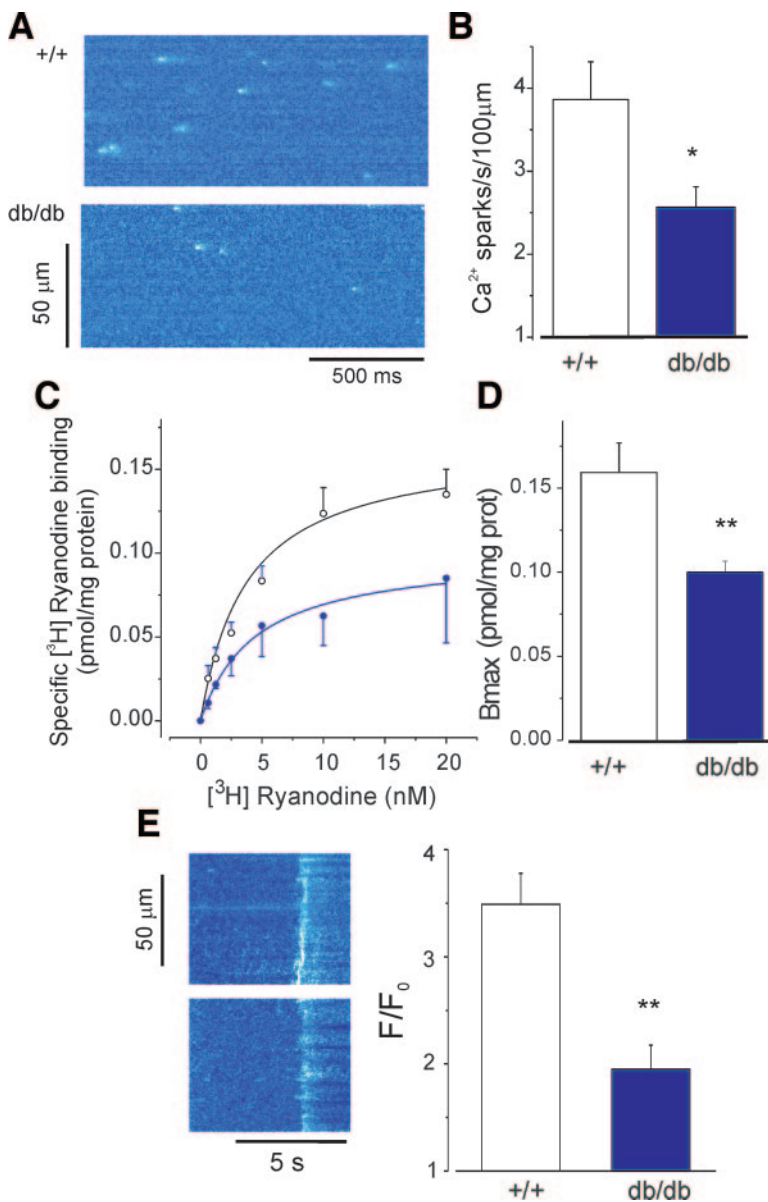


FIG. 4. Ca^{2+} spark occurrence is decreased in *db/db* hearts, along with a reduction in RyR expression. **A:** Line-scan images showing spontaneous Ca^{2+} sparks recorded in *+/+* and *db/db* permeabilized myocytes. **B:** Ca^{2+} sparks per second per 100 μm recorded in 10 *+/+* and in 14 *db/db* myocytes. **C:** Specific [^3H]ryanodine binding measured in *+/+* (open circles) and *db/db* (blue circles) hearts. Lines represent fitting of the points with the equation $B = B_{\text{max}} \times [\text{ryanodine}] / (K_d + [\text{ryanodine}])$ with B as the specific binding. **D:** Averaged B_{max} calculated for six *+/+* and six *db/db* hearts. **E:** **Left,** line-scan images recorded in *+/+* (top) and *db/db* (bottom) permeabilized myocytes during 20 mmol/l caffeine application. **Right,** averaged peak fluorescence ratio (measured as F/F_0 as in Fig. 1) obtained during caffeine application in *+/+* ($n = 20$) and *db/db* myocytes ($n = 20$). * $P < 0.05$; ** $P < 0.01$.

DISCUSSION

Cardiovascular alterations constitute the most frequent cause of death in diabetic patients (3–5). At present, an integrated scheme of excitation-contraction coupling alterations in type 2 diabetic hearts is incomplete. Our study of *db/db* mice, which experiences obesity-associated type 2 diabetes, shows that the contractile dysfunction linked with the cardiomyopathy can be explained, at least in part, by disturbed Ca^{2+} cycling, i.e., reduced Ca^{2+} influx via L-type Ca^{2+} channels, lowered Ca^{2+} release from sarcoplasmic reticulum, slowed Ca^{2+} reuptake, and increased Ca^{2+} efflux.

db/db mice exhibit cardiac failure that is evident as early as 12 weeks of age (29). Here, we used 15-week-old *db/db* mice and confirmed the depression of systolic function by M-mode echocardiography (Fig. 1A and B). Systolic dysfunction is accompanied by a dramatic decrease of cellular $[\text{Ca}^{2+}]_i$ transients recorded in whole hearts (Fig. 1G) and isolated field-stimulated (11) and patch-clamped myocytes (Fig. 2A). This depression of Ca^{2+} release could underlie the systolic dysfunction of *db/db* hearts, although other

factors (e.g., contractile myofibrils and elastic properties of the heart) may contribute.

The simultaneous recording of cell shortening, $[\text{Ca}^{2+}]_i$ transient and I_{Ca} in isolated *db/db* myocytes revealed that cell contraction is decreased without an apparent decrease in excitation-contraction coupling efficiency (Fig. 2E). The cellular contractile dysfunction is consistent with the echocardiographic measurements presented in Fig. 1. Furthermore, the amplitude of the $[\text{Ca}^{2+}]_i$ transient recorded in isolated cells was reduced (Fig. 2C), which is consistent with data obtained by two-photon microscopy in whole hearts (Fig. 1). Interestingly, the trigger I_{Ca} was also reduced in *db/db* myocytes (Fig. 2D), thereby imposing a limitation on the amount of Ca^{2+} ions entering into diabetic myocytes. This limitation is likely exacerbated by the shift of I_{Ca} activation curve toward more depolarized potentials, which results in a reduction of the “window current.” Given the fact that the activity of single L-type Ca^{2+} channels is not modified and that the reduction in the density of pore-forming subunit $\alpha_1\text{c}$ is similar to the reduction in whole-cell I_{Ca} , it is likely that the reduction in

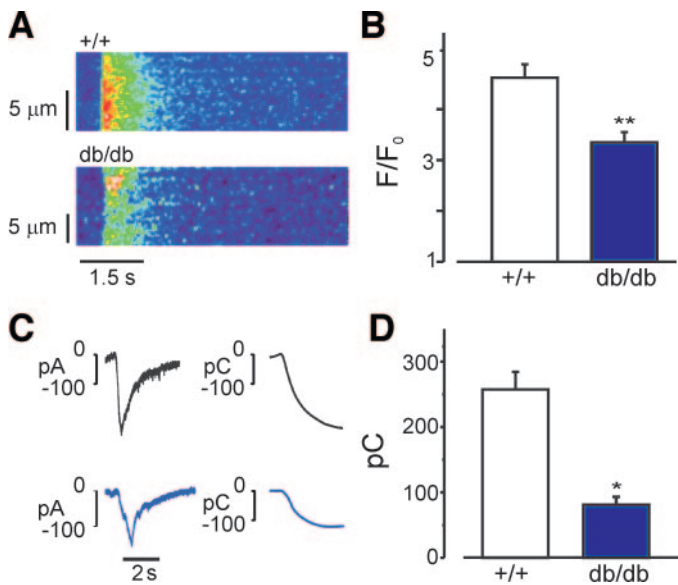


FIG. 5. Sarcoplasmic reticulum Ca^{2+} load is decreased in *db/db* cardiomyocytes. **A:** Caffeine-evoked $[\text{Ca}^{2+}]_i$ transients in a +/+ and *db/db* myocyte. **B:** Averaged peak fluorescence ratio (F/F_0 , as in Fig. 1) in +/+ ($n = 35$) and *db/db* ($n = 32$) myocytes. **C:** I_{NCX} evoked by caffeine (left) and its running integral (right) recorded in a +/+ (top) and a *db/db* (bottom) myocyte. **D:** Averaged integral of the I_{NCX} recorded during caffeine application in +/+ ($n = 6$) and *db/db* ($n = 6$) myocytes. * $P < 0.01$; ** $P < 0.001$.

I_{Ca} is the result of fewer L-type Ca^{2+} channels in *db/db* mice hearts. A decrease in $[\text{Ca}^{2+}]_i$ transient has been found in other models of cardiac pathology and contractile dysfunction (rev. in 27), but in most cases, cardiac hypertrophy and normal I_{Ca} density accompany the depressed $[\text{Ca}^{2+}]_i$ transient. In the case of type 2 diabetic mice, a systematic reduction of I_{Ca} (Fig. 2D) may underlie the decreased sarcoplasmic reticulum Ca^{2+} release and contraction either directly, by triggering lower Ca^{2+} release, or indirectly, by lowering the sarcoplasmic reticulum Ca^{2+} load. Under a reduced I_{Ca} , a new equilibrium may be reached in diabetic hearts where Ca^{2+} entry, release, and uptake are reduced. The reduction in sarcoplasmic reticulum Ca^{2+} load may also be due to a depression in SERCA2a activity. In fact, we found the $[\text{Ca}^{2+}]_i$ transient to decay slower in *db/db* myocytes. In mice, decline of the $[\text{Ca}^{2+}]_i$ transient is mainly (~90%) due to SERCA2a activity, with relatively minor contribution (~9%) by the NCX (30). Thus slowing of the $[\text{Ca}^{2+}]_i$ transient in *db/db* is most likely caused by decreased SERCA activity. In support of this notion, others have shown a large increase in the expression of the SERCA inhibiting protein phospholamban in *db/db* hearts (11). Moreover, the increased Ca^{2+} efflux through the NCX can contribute to decreasing the sarcoplasmic reticulum Ca^{2+} load.

RyR activity can be determined by examining Ca^{2+} sparks. We found that *db/db* cardiac myocytes exhibit reduced rate of Ca^{2+} spark frequency (Fig. 4A and B). This reduction cannot be explained by changes in diastolic $[\text{Ca}^{2+}]_i$ (11) or I_{Ca} (Fig. 3) because Ca^{2+} sparks were recorded in permeabilized myocytes, where internal $[\text{Ca}^{2+}]$ is fixed and I_{Ca} is absent. However, permeabilization may wash out soluble components with capacity to modulate RyRs (Na^+ , Mg^{2+} , sorcin...) that may be altered in *db/db* myocytes. The decreased Ca^{2+} spark frequency may instead be an indication of depressed expression of RyRs (Fig. 4C and D) and/or the sarcoplasmic reticulum

Ca^{2+} load (Fig. 4E). The decrease in RyR abundance is consistent with data obtained in type 1 diabetic hearts (31–34), although in type 2 diabetes, no change in RyR expression was found in two previous studies (9,11). A decrease in the frequency of spontaneous Ca^{2+} sparks could have a beneficial effect by preventing Ca^{2+} leakage from the sarcoplasmic reticulum and enhancing the sarcoplasmic reticulum Ca^{2+} load (18), analogous to effects seen with FKBP12.6 overexpression (35). But because sarcoplasmic reticulum Ca^{2+} load was decreased in *db/db* myocytes (Fig. 4E), this suggests that defects concomitant to reduced RyR expression contribute to altered Ca^{2+} cycling in *db/db* mice hearts.

This study has been performed in type 2 diabetic mice with obesity, which recapitulate human pathology. However, even if animal models are a valuable resource to elucidate molecular mechanisms of human pathology, there are clear limitations to translate results from bench to bedside. For example, the heart rate in mice is higher than in humans, so the relative contribution of SERCA2 over NCX is notably different (30).

In conclusion, we have identified impaired Ca^{2+} -induced Ca^{2+} release in obesity-linked type 2 diabetes that underlies depressed cardiac function. A general reduction in the membrane permeability to Ca^{2+} was identified. Because less Ca^{2+} enters the cell through I_{Ca} , less Ca^{2+} is released through RyRs. This is due to a reduction in both sarcolemmal Ca^{2+} channels and sarcoplasmic reticulum Ca^{2+} release channels expression.

ACKNOWLEDGMENTS

H.H.V. has received National Institutes of Health Grant HL55438. L.P. has received a travel grant from Deutscher Akademischer Austausch Dienst. S.R. and A.M.G. are Centre National de la Recherche Scientifique scientists. The project was funded by Institute National de la Santé et la Recherche Médicale, Université de Montpellier 1, Servier Laboratories, and Programme Nationale de Recherche.

We thank Nancy Benkuski, Georgina Gurrola, and Patrice Bideaux for excellent technical assistance. We also thank Prof. M. Dautzat for advice with echocardiography.

REFERENCES

1. Taegtmeier H, McNulty P, Young ME: Adaptation and maladaptation of the heart in diabetes: Part I. General concepts. *Circulation* 105:1727–1733, 2002
2. Schaffer SW: Cardiomyopathy associated with noninsulin-dependent diabetes. *Mol Cell Biochem* 107:1–20, 1991
3. Bell DSH: Heart failure: the frequent, forgotten, and often fatal complication of diabetes. *Diabetes Care* 26:2433–2441, 2003
4. Bauters C, Lambin N, Mc Fadden EP, Van Belle E, Millaire A, De Groote P: Influence of diabetes mellitus on heart failure risk and outcome. *Cardiovasc Diabetol* 2: 1, 2003
5. Laakso M: Hyperglycemia and cardiovascular disease in type 2 diabetes. *Diabetes* 48:937–942, 1999
6. Regan TJ, Khan MI, Jesrani MU, Oldewurtel HA, Ettinger PO: Alterations of myocardial function and metabolism in chronic diabetes mellitus. *Recent Adv Stud Cardiac Struct Metab* 3:169–178, 1973
7. Penpargkul S, Schaible T, Yipintsoi T, Scheuer J: The effect of diabetes on performance and metabolism of rat hearts. *Circ Res* 47:911–921, 1980
8. Fein F, Kornstein L, Strobeck J, Capasso J, Sonnenblick E: Altered myocardial mechanics in diabetic rats. *Circ Res* 47:922–933, 1980
9. Misra T, Gilchrist JSC, Russell JC, Pierce GN: Cardiac myofibrillar and sarcoplasmic reticulum function are not depressed in insulin-resistant JCR:LA-cp rats. *Am J Physiol Heart Circ Physiol* 276:H1811–H1817, 1999
10. Abe T, Ohga Y, Tabayashi N, Kobayashi S, Sakata S, Misawa H, Tsuji T, Kohzaki H, Suga H, Taniguchi S, Takaki M: Left ventricular diastolic dysfunction in type 2 diabetes mellitus model rats. *Am J Physiol Heart Circ Physiol* 282:H138–H148, 2002

11. Belke DD, Swanson EA, Dillmann WH: Decreased sarcoplasmic reticulum activity and contractility in diabetic *db/db* mouse heart. *Diabetes* 53:3201–3208, 2004
12. Schaffer SW, Allo S, Punna S, White T: Defective response to cAMP-dependent protein kinase in non-insulin-dependent diabetic heart. *Am J Physiol* 261:E369–E376, 1991
13. Allo SN, Lincoln TM, Wilson GL, Green FJ, Watanabe AM, Schaffer SW: Non-insulin-dependent diabetes-induced defects in cardiac cellular calcium regulation. *Am J Physiol* 260:C1165–C1171, 1991
14. Belke DD, Larsen TS, Gibbs EM, Severson DL: Altered metabolism causes cardiac dysfunction in perfused hearts from diabetic (*db/db*) mice. *Am J Physiol Endocrinol Metab* 279:E1104–E1113, 2000
15. Bénitah J-P, Perrier E, Gómez AM, Vassort G: Effects of aldosterone on transient outward K⁺ current density in rat ventricular myocytes. *J Physiol (Lond)* 537:151–126, 2001
16. Rubart M, Wang E, Dunn KW, Field LJ: Two-photon molecular excitation imaging of Ca²⁺ transients in Langendorff-perfused mouse hearts. *Am J Physiol Cell Physiol* 284:C1654–C1668, 2003
17. Gómez AM, Kerfant BG, Vassort G: Microtubule disruption modulates Ca(2+) signaling in rat cardiac myocytes. *Circ Res* 86:30–36, 2000
18. Overend CL, Eisner DA, O'Neill SC: The effect of tetracaine on spontaneous Ca²⁺ release and sarcoplasmic reticulum calcium content in rat ventricular myocytes. *J Physiol (Lond)* 502:471–479, 1997
19. Farrell EF, Antaramián A, Rueda A, Gómez AM, Valdivia HH: Sorcin inhibits calcium release and modulates excitation-contraction coupling in the heart. *J Biol Chem* 278:34660–34666, 2003
20. Heredia Mdel P, Delgado C, Pereira L, Perrier R, Richard S, Vassort G, Benitah JP, Gomez AM: Neuropeptide Y rapidly enhances [Ca(2+)](i) transients and Ca(2+) sparks in adult rat ventricular myocytes through Y(1) receptor and PLC activation. *J Mol Cell Cardiol* 38:205–212, 2005
21. Foerster K, Groner F, Matthes J, Koch WJ, Birnbaumer L, Herzig S: Cardioprotection specific for the G protein Gi2 in chronic adrenergic signaling through beta 2-adrenoceptors. *Proc Natl Acad Sci U S A* 100:14475–14480, 2003
22. Schroder F, Handrock R, Beuckelmann DJ, Hirt S, Hullin R, Priebe L, Schwinger RH, Weil J, Herzig S: Increased availability and open probability of single L-type calcium channels from failing compared with nonfailing human ventricle. *Circulation* 98:969–976, 1998
23. Lokuta AJ, Meyers MB, Sander PR, Fishman GI, Valdivia HH: Modulation of cardiac ryanodine receptors by sorcin. *J Biol Chem* 272:25333–25338, 1997
24. Perrier E, Kerfant BG, Lalevee N, Bideaux P, Rossier MF, Richard S, Gómez AM, Bénitah JP: Mineralocorticoid receptor antagonism prevents the electrical remodeling that precedes cellular hypertrophy after myocardial infarction. *Circulation* 110:776–783, 2004
25. Solaro RJ, Rarick HM: Troponin and tropomyosin: proteins that switch on and tune in the activity of cardiac myofilaments. *Circ Res* 83:471–480, 1998
26. Cheng H, Lederer WJ, Cannell MB: Calcium sparks: elementary events underlying excitation-contraction coupling in heart muscle. *Science* 262:740–744, 1993
27. Bénitah JP, Kerfant BG, Vassort G, Richard S, Gómez AM: Altered communication between L-type calcium channels and ryanodine receptors in heart failure. *Front Biosci* 7:e263–e275, 2002
28. Gómez AM, Schwaller B, Porzig H, Vassort G, Niggli E, Egger M: Increased exchange current but normal Ca²⁺ transport via Na⁺-Ca²⁺ exchange during cardiac hypertrophy after myocardial infarction. *Circ Res* 91:323–330, 2002
29. Semeniuk LM, Kryski AJ, Severson DL: Echocardiographic assessment of cardiac function in diabetic *db/db* and transgenic *db/db*-hGLUT4 mice. *Am J Physiol Heart Circ Physiol* 283:H976–H982, 2002
30. Bers DM: *Excitation-Contraction Coupling and Cardiac Contractile Force*. Dordrecht, the Netherlands, Kluwer Academic Publishers, 2001
31. Yu Z, Tibbits GF, McNeill JH: Cellular functions of diabetic cardiomyocytes: contractility, rapid-cooling contracture, and ryanodine binding. *Am J Physiol* 266:H2082–H2089, 1994
32. Netticadan T, Tamsah RM, Kent A, Elimban V, Dhalla NS: Depressed levels of Ca²⁺-cycling proteins may underlie sarcoplasmic reticulum dysfunction in the diabetic heart. *Diabetes* 50:2133–2138, 2001
33. Bidasee KR, Nallani K, Henry B, Dincer UD, Besch HR Jr: Chronic diabetes alters function and expression of ryanodine receptor calcium-release channels in rat hearts. *Mol Cell Biochem* 249:113–123, 2003
34. Guner S, Arioglu E, Tay A, Tasdelen A, Aslamaci S, Bidasee KR, Dincer UD: Diabetes decreases mRNA levels of calcium-release channels in human atrial appendage. *Mol Cell Biochem* 263:143–150, 2004
35. Gómez AM, Schuster I, Fauconnier J, Prestle J, Hasenfuss G, Richard S: FKBP12.6 overexpression decreases Ca²⁺ spark amplitude but enhances [Ca²⁺]_i transient in rat cardiac myocytes. *Am J Physiol Heart Circ Physiol* 287:H1987–H1993, 2004